


Locus Coeruleus Shows a Spatial Pattern of Structural Disintegration in Parkinson's Disease

Christopher F. Madelung, MD,^{1,2*}  David Meder, PhD,¹ Søren A. Fuglsang, PhD,¹ Marta M. Marques, MD,¹ Vincent O. Boer, PhD,¹ Kristoffer H. Madsen, PhD,^{1,3} Esben T. Petersen, PhD,^{1,4} Anne-Mette Hejl, MD, PhD,^{2,5} Annemette Løkkegaard, MD, PhD,^{2,5} and Hartwig R. Siebner, MD, DMSci^{1,2,5*}

¹Danish Research Centre for Magnetic Resonance, Centre for Functional and Diagnostic Imaging and Research, Copenhagen University Hospital Amager and Hvidovre, Copenhagen, Denmark

²Department of Neurology, Copenhagen University Hospital Bispebjerg and Frederiksberg, Copenhagen, Denmark

³Department of Applied Mathematics and Computer Science, Technical University of Denmark, Kgs. Lyngby, Denmark

⁴Department of Health Technology, Technical University of Denmark, Kgs. Lyngby, Denmark

⁵Department of Clinical Medicine, University of Copenhagen, Copenhagen, Denmark

ABSTRACT: Background: Parkinson's disease (PD) causes a loss of neuromelanin-positive, noradrenergic neurons in the locus coeruleus (LC), which has been implicated in nonmotor dysfunction.

Objectives: We used "neuromelanin sensitive" magnetic resonance imaging (MRI) to localize structural disintegration in the LC and its association with nonmotor dysfunction in PD.

Methods: A total of 42 patients with PD and 24 age-matched healthy volunteers underwent magnetization transfer weighted (MTw) MRI of the LC. The contrast-to-noise ratio of the MTw signal (CNR_{MTw}) was used as an index of structural LC integrity. We performed slice-wise and voxelwise analyses to map spatial patterns of structural disintegration, complemented by principal component analysis (PCA). We also tested for correlations between regional CNR_{MTw} and severity of nonmotor symptoms.

Results: Mean CNR_{MTw} of the right LC was reduced in patients relative to controls. Voxelwise and slice-wise analyses showed that the attenuation of CNR_{MTw} was confined to the

right mid-caudal LC and linked regional CNR_{MTw} to non-motor symptoms. CNR_{MTw} attenuation in the left mid-caudal LC was associated with the orthostatic drop in systolic blood pressure, whereas CNR_{MTw} attenuation in the caudal most portion of right LC correlated with apathy ratings. PCA identified a bilateral component that was more weakly expressed in patients. This component was characterized by a gradient in CNR_{MTw} along the rostro-caudal and dorso-ventral axes of the nucleus. The individual expression score of this component reflected the overall severity of nonmotor symptoms.

Conclusion: A spatially heterogeneous disintegration of LC in PD may determine the individual expression of specific nonmotor symptoms such as orthostatic dysregulation or apathy. © 2022 The Authors. *Movement Disorders* published by Wiley Periodicals LLC on behalf of International Parkinson Movement Disorder Society.

Key Words: Parkinson's disease; locus coeruleus; MRI; non-motor; noradrenaline

Parkinson's disease (PD) leads to a wide range of nonmotor symptoms, including sleep disturbances, depression, anxiety, apathy, cognitive impairment, and

autonomic dysfunction.¹ Orthostatic hypotension is a prevalent autonomic symptom affecting 30% to 58% of patients with PD.² Apathy and depressive symptoms

This is an open access article under the terms of the Creative Commons Attribution-NonCommercial License, which permits use, distribution and reproduction in any medium, provided the original work is properly cited and is not used for commercial purposes.

***Correspondence to:** Dr. Christopher F. Madelung, Danish Research Centre for Magnetic Resonance, Copenhagen University Hospital Amager and Hvidovre, Kettegaard Allé 30, 2650 Hvidovre, Denmark, E-mail: christopherfm@drcmr.dk; or Dr. Hartwig R. Siebner, Danish Research Centre for Magnetic Resonance, Copenhagen University Hospital Amager and Hvidovre, Kettegaard Allé 30, 2650 Hvidovre, Denmark, E-mail: hartwig@drcmr.dk

Relevant conflicts of interest/financial disclosures: H.R.S. has received honoraria as speaker from Sanofi Genzyme, Denmark, and

Novartis, Denmark; as consultant from Sanofi Genzyme, Denmark, Lophora, Denmark, and Lundbeck AS, Denmark; and as editor-in-chief (*Neuroimage Clinical*) and senior editor (*NeuroImage*) from Elsevier Publishers, Amsterdam, the Netherlands. H.R.S. has received royalties as book editor from Springer Publishers, Stuttgart, Germany, and from Gyldendal Publishers, Copenhagen, Denmark. A.L. has received honoraria as speaker from AbbVie, USA, and GE Healthcare, Denmark. The other authors have nothing to report.

Received: 25 September 2021; **Revised:** 30 November 2021; **Accepted:** 27 December 2021

Published online 3 February 2022 in Wiley Online Library (wileyonlinelibrary.com). DOI: 10.1002/mds.28945

are also frequent in PD, with a prevalence of approximately 40% and 35%, respectively.^{3,4} The locus coeruleus (LC) is a paired nucleus in the dorsolateral pontine tegmentum consisting of approximately 50,000 pigmented noradrenergic neurons^{5,6} that plays a role in the regulation of sleep and arousal, executive function, memory consolidation, motivation, and decision making as well as autonomic function.^{7,8} In PD, the LC is severely affected by the progressive accumulation of Lewy bodies and neurodegeneration,^{9,10} and neurodegeneration of the LC has been linked to nonmotor symptoms such as rapid eye movement sleep behavior disorder (RBD), mild cognitive impairment, depression, and orthostatic hypotension.¹¹⁻¹⁶

The LC was traditionally viewed as a unitary nucleus processing the same type of information across its structure, distributing a uniform message across its efferent projections.^{7,17} More recent research has revealed a topographical organization of neurons based on target structures with forebrain projecting neurons located rostrally and neurons projecting to the basal ganglia, cerebellum, and spinal cord located in the middle and caudal parts of the nucleus^{18,19} with corresponding functional modules across the structure.⁷ Yet, there is to date little information on whether neurodegeneration in PD affects the LC in a uniform manner.

Neuromelanin-sensitive magnetic resonance imaging (MRI) has been introduced as a sensitive means of assessing PD-related changes in the substantia nigra and LC.²⁰⁻²³ Neuromelanin MRI renders the LC visible as a paired, elongated, hyperintense structure along the floor of the fourth ventricle in the upper pons, and voxel intensities have been shown to be closely associated with the number of neuromelanin-rich neurons in the LC.²⁴ Recently, magnetization transfer weighted (MTw) imaging was introduced, providing better LC contrast-to-noise ratio (CNR) compared with conventional turbo spin echo sequences.²⁵ A recent study investigating LC integrity in PD using MTw MRI showed spatial inhomogeneity in the pattern of neurodegeneration with decreased CNR in the caudal part of the nucleus, but not in middle or rostral parts.²³

Here, we used ultra-high-field (7 tesla [T]) MTw MRI to investigate the extent of LC neurodegeneration in PD at high spatial resolution and its relationship with nonmotor symptoms.

We hypothesized that patients would show a reduced MTw signal in the LC reflecting the neuronal loss of noradrenergic neurons. We expected the signal reduction in the LC to scale with the severity of nonmotor symptoms. Furthermore, we explored the spatial resolution of 7T MRI to identify spatial gradients of structural disintegration and how they are related to nonmotor symptoms.

Methods

Participants

We recruited 49 patients with PD and 27 healthy, age-matched controls (HCs) as part of a larger study investigating brainstem changes in PD. Seven patients were excluded because of contraindications to MRI,³ unreported neurological conditions,¹ incidental findings,¹ and poor scan quality.² Three HCs were excluded because of unreported neurological conditions² and poor scan quality.¹ Patients were recruited from the Movement Disorders outpatient clinic at the Department of Neurology, Copenhagen University Hospital Bispebjerg (Copenhagen, Denmark) and private practice neurology clinics based in the Copenhagen region. All participants in the PD group were required to have a clinical diagnosis of PD assessed by a neurologist and to fulfill the Movement Disorder Society clinical diagnostic criteria for “clinically established PD” or “clinically probable PD”.²⁶ Exclusion criteria were pregnancy or breastfeeding, history of other neurologic or psychiatric diseases, pacemaker or other implanted electronic devices, and claustrophobia. The PD group spanned a large range in terms of disease duration (0–17 years) and time since symptom onset (1–18 years) and included patients with mild to moderate disease (Hoehn and Yahr stages 1–3). HCs were recruited by online advertisements, were required to be aged 18 years or older with no history of neurologic or psychiatric disease, and did not fulfill any of the exclusion criteria mentioned previously.

The study was approved by the Regional Committee on Health Research Ethics of the Capital Region of Denmark (record identification: H-18021857). All participants gave their written informed consent to participate in the study. The study was preregistered at ClinicalTrials.gov (identifier: NCT03866044).

Study Procedures

Participants underwent a neurological examination to exclude participants exhibiting symptoms of any neurological condition other than PD. Patients' motor and nonmotor symptom severity was assessed in the *on* state (on their usual dopaminergic treatment) using the Unified Parkinson's Disease Rating Scale (UPDRS) and the Non-Motor Symptom Scale (NMSS).^{27,28} Patients' blood pressure was measured in the supine position following a 5-minute rest period after which a series of consecutive measurements were made for a period of 3 minutes upon standing up.²⁹ The maximum change in systolic blood pressure was recorded as a measure of orthostatic hypotension. Apathy and depression were assessed in all participants using the Lille Apathy Rating Scale (LARS) and Beck's Depression Inventory-II (BDI-II).³⁰⁻³³ In addition, we registered age and sex as

well as patients' disease duration, time since onset of motor symptoms, and medication status.

Magnetic Resonance Imaging

MRI of the brain was performed with a Philips Achieva 7T scanner (Philips, Best, the Netherlands) equipped with a 32-channel Nova head coil (Nova Medical Inc., Wilmington, MA). We scanned patients in the *on* medication state to limit tremor-related movement. Dyskinesia was not observed in any of the patients during the scanning session. We acquired T1-weighted (T1w), high-resolution (1-mm isotropic) magnetization prepared rapid gradient echo images with a field of view covering the entire head (200 × 288 × 288 voxels), echo time/repetition time = 2.2/4.9 milliseconds, and acquisition time = 3:30 minutes. To assess the integrity of the LC, we acquired MTw images using a three-dimensional, high-resolution (voxel size, 0.4 × 0.4 × 1.0 mm) ultra-fast gradient echo sequence aligned to the anterior commissure-posterior commissure (AC-PC) line with a field of view covering the midbrain and rostral pons (640 × 640 × 34 voxels), echo time/repetition time = 4.1/8.1 milliseconds, flip angle = 7 degrees, two averages. Magnetization transfer saturation was achieved by applying 16 block-shaped prepulses at a

frequency offset of 2 kHz (flip angle = 278 degrees, duration = 10 milliseconds), acquisition time = 8 minutes. We also acquired T1w images with identical acquisition parameters for coregistration purposes, but with a zero-degree flip angle for the off-resonance prepulses.

Image Processing

Postprocessing of the MRI data and calculation of CNR maps followed the procedure described in a recent study with healthy participants.³⁴

Using the Advanced Normalization Tools (ANTs) software (<http://stnava.github.io/ANTs/>), images were first corrected for low-frequency spatial intensity inhomogeneities, coregistered and subsequently normalized to template space by rigid-body, affine, and nonlinear registration.³⁵ High-resolution images were transformed to individual participants' T1w space for evaluation of registration accuracy. T1w reference images were normalized to a study-specific T1w template and finally to the Montreal Neurological Institute (MNI) 0.5-mm International Consortium for Brain Mapping (ICBM) 152 T1w asymmetric template³⁶ by rigid-body, affine, and nonlinear registration. Finally, MTw and T1w images were transformed to MNI template space

TABLE 1 Demographics of the study population

	Healthy, age-matched controls (n = 24)	Patients with Parkinson's disease (n = 42)	P value
Sex, male/female	16/8	23/19	0.493
Age, years	71.5 (43.0–80.0)	67.5 (38.0–84.0)	0.557
Handedness, left/right/ambidextrous	4/20/0	2/39/1	0.180
Disease duration, years	–	3.66 (0.250–17.3)	–
Time since symptom onset, years	–	6.06 (0.980–18.3)	–
Modified Hoehn and Yahr stage	–	2 (1–3)	–
Levodopa equivalent dose, mg/day	–	479 (100–2140)	–
Most affected side, right/left	–	17/25	–
UPDRS-III	–	23.4 ± 9.27	–
NMSS	–	31 (3–118)	–
MoCA	28 (23–30)	28 (17–30)	0.393
BDI-II	3 (0–11)	8 (0–20)	0.001
LARS	–25.5 ± 4.93	–22.4 ± 6.09	0.028
	Range (–33 to –14)	Range (–32 to –7)	

Data are given as n, mean ± standard deviation, or median (range). Between-group differences was assessed using the Student *t* test for normally distributed data and the Wilcoxon rank-sum test when normal distribution could not be assumed. Between-group differences in sex distribution and handedness were assessed using Pearson's chi-squared test with Yates' continuity correction and Fisher's exact test, respectively.

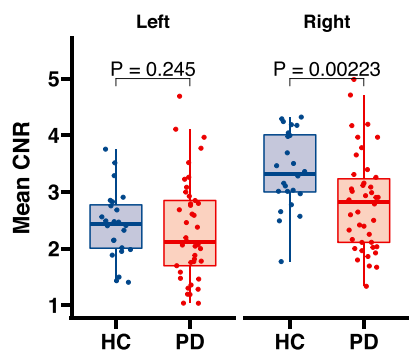
Abbreviations: UPDRS-III, Unified Parkinson's Disease Rating Scale Part III; NMSS, Non-Motor Symptom Scale; MoCA, Montreal Cognitive Assessment; BDI-II, Beck's Depression Inventory II; LARS, Lille Apathy Rating Scale.

by combining the transformation parameters obtained from within-subject coregistration with the transformation parameters and warp field obtained from the normalization steps.

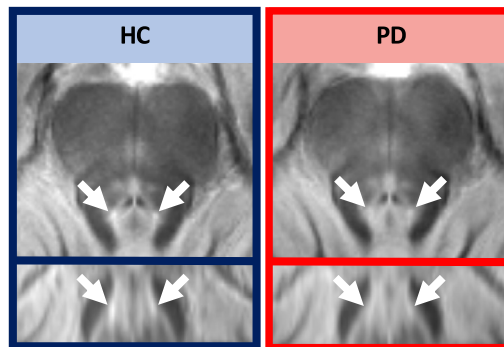
CNR_{MTw} maps were calculated from normalized MTw images by subtracting the mean signal intensity (SI) of a 4 × 4 × 4 mm cubic reference region placed centrally in the pontine tegmentum (PT_{ref}) and dividing by the standard deviation (sd) of this reference region: CNR_{MTw} = (SI - mean_{PT_{ref}})/sd_{PT_{ref}}. We chose to quantify LC contrast relative to the standard deviation of the reference region instead of the mean signal as the standard deviation provides a better estimate of the noise in the imaging data.³⁴

A region of interest (ROI) for the LC was defined based on a probabilistic LC atlas constructed from 7T MTw images from 53 healthy participants (age range, 52–84 years; mean, 66 years).³⁴ The liberal version of this atlas (5% probability) was chosen to allow for interindividual difference of the spatial extent of the LC. Because the atlas also included hyperintense voxels forming the border of the fourth ventricle, we created a binary mask applying threshold-based segmentation of the brainstem using the MNI 0.5-mm ICBM152 T1w, nonlinear, asymmetric template. We effectively excluded hyperintense border voxels by masking out voxels outside the segmented brainstem (Supplementary Fig. S1). Mean CNR_{MTw} was

A. Group difference in overall LC CNR.



B. Group average (MT-weighted images).



C. Correlations with non-motor symptom severity.

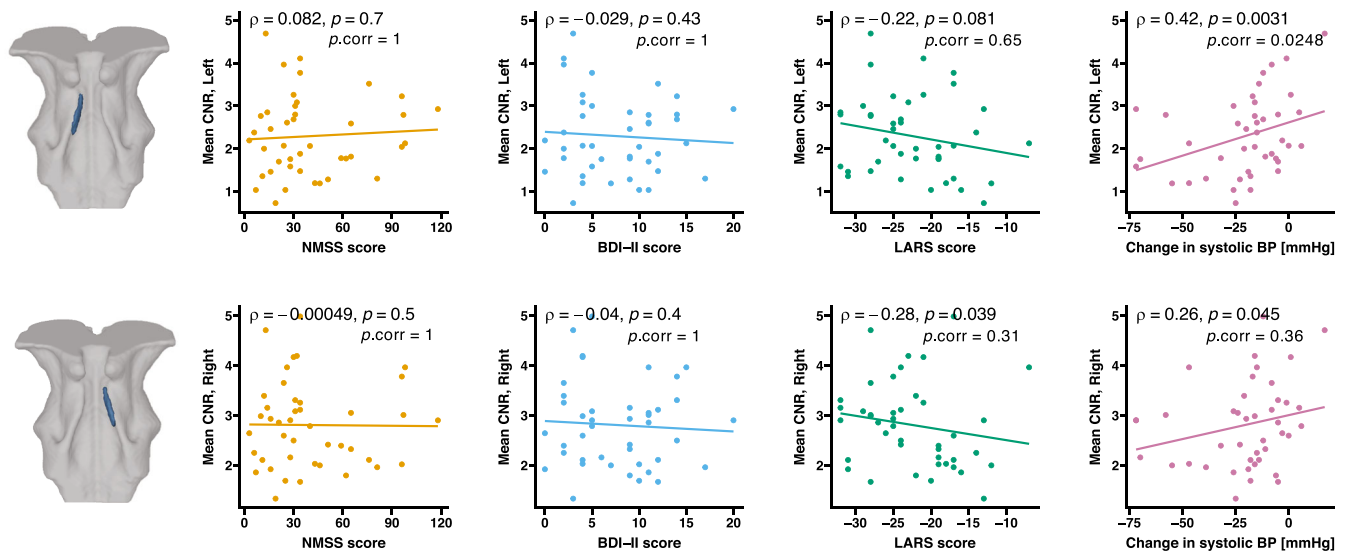


FIG. 1. Overall group difference in LC CNR_{MTw} and correlations with nonmotor symptom severity. Patients had lower mean CNR_{MTw} in the right LC compared with age-matched healthy volunteers, $t_{57,2} = -2.96$ ($P = 0.002$) (A). The reduction in CNR_{MTw} is visualized in group average MTw maps (B). Mean CNR_{MTw} of the left LC correlated with orthostatic change in systolic BP. No significant correlations were found for overall nonmotor symptom severity (NMSS), depressive symptoms (BDI-II score), or apathy (LARS) following multiple comparisons correction (C). BDI-II, Beck's Depression Inventory II; BP, blood pressure; CNR, contrast-to-noise ratio; CNR_{MTw}, contrast-to-noise ratio of the magnetization transfer weighted signal; HC, healthy, age-matched controls; LARS, Lille Apathy Rating Scale; LC, locus coeruleus; MT, magnetization transfer; MTw, magnetization transfer weighted signal; NMSS, Non-Motor Symptom Scale; PD, Parkinson's disease. [Color figure can be viewed at wileyonlinelibrary.com]

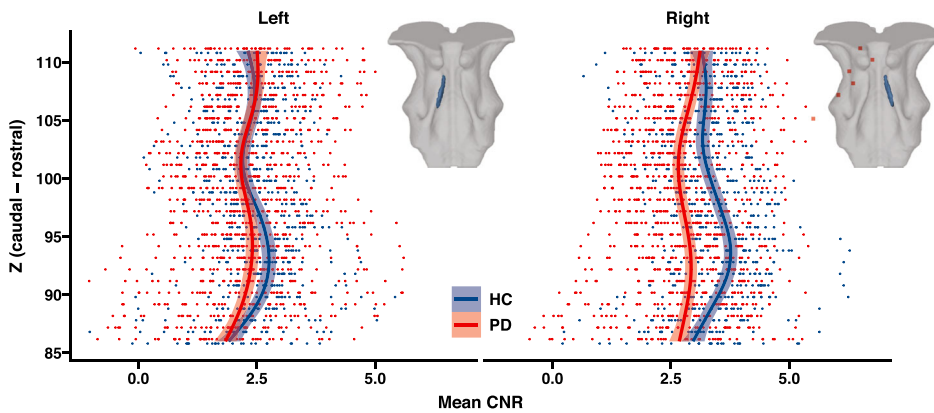
extracted from the masked bilateral LC ROI as well as from every slice from the rostral to the caudal most extent of the LC ROI in the z-direction for each side separately.

Statistical Analyses

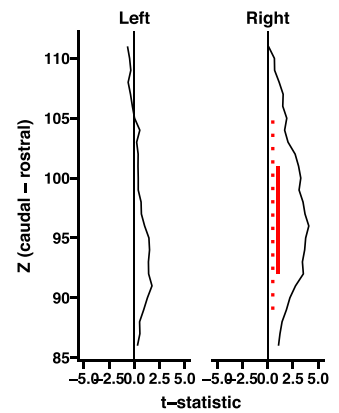
Statistical analyses were performed using R (version 4.0.4; R Foundation for Statistical Computing, Vienna, Austria) and Python (version 3.7.9; Python Software Foundation, Wilmington, DE). Between-group differences were tested using independent-samples *t* tests of mean CNR_{MTW} values of right and left LC, mean CNR_{MTW} values of left and right LC per slice, and single-voxel CNR_{MTW} values. One-tailed correlation analyses were performed to test our hypotheses that LC

CNR would correlate negatively with overall nonmotor symptom severity (NMSS), apathy (LARS), and depression (BDI-II) and positively with an orthostatic drop in systolic blood pressure in patients. Correlations were assessed for the mean CNR_{MTW} of bilateral LC and slice-wise and voxel-wise CNR_{MTW}-values to explore at which rostro-caudal levels CNR_{MTW} attenuation was associated with nonmotor symptom severity. One-tailed Pearson's product moment correlation coefficient and one-tailed Spearman's rho were calculated as appropriate. Statistical significance was accepted at a threshold of *P* < 0.05 family-wise error (FWE) corrected. Cluster-level inference was used to explore the spatial extent of between-group differences and correlations with nonmotor symptom severity. After images had been upsampled and normalized to 0.5-mm template space,

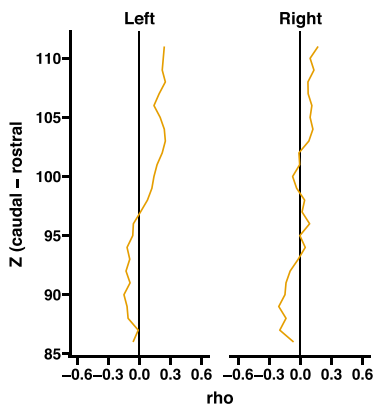
A. Slice-wise contrast-to-noise ratio.



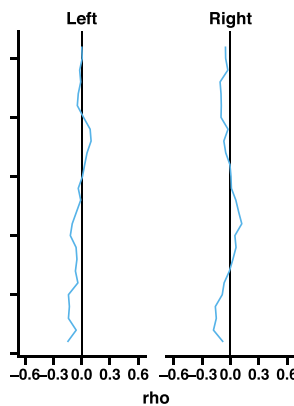
B. Group difference.



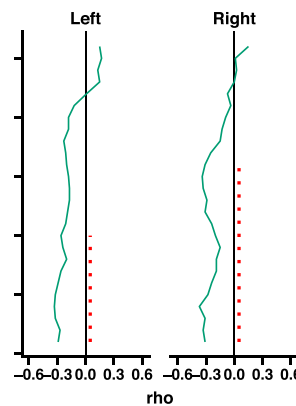
C. NMSS



D. BDI-II



E. LARS



F. Change in systolic BP

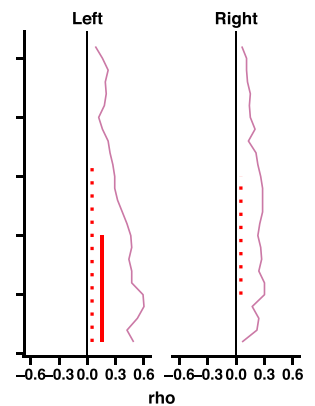


FIG. 2. Rostro-caudal, slice-wise differences in LC CNR_{MTW} and correlations with nonmotor symptom severity. **(A)** By extracting the slice-wise LC CNR_{MTW} along the rostro-caudal extent of the nucleus, we found lower CNR_{MTW} values in the caudal part of the right LC in patients with PD. Groupwise average CNR_{MTW} values are visualized by fitting a local polynomial regression function. **(B)** Per-slice *t* statistic and significance level are presented. Red bar indicates slices at which CNR_{MTW} was significantly lower (family-wise error [FWE]-adjusted *P* < 0.05). LC CNR_{MTW} values were found to correlate with **(E)** apathy and **(F)** orthostatic hypotension. Red bars indicate slices at which CNR_{MTW} correlated with the severity of nonmotor symptoms (dashed = unadjusted *P* < 0.05, solid = FWE-adjusted *P* < 0.05). No correlations were observed for NMSS **(C)** or BDI-II scores **(D)**. BDI-II, Beck's Depression Inventory II; BP, blood pressure; CNR, contrast-to-noise ratio; CNR_{MTW}, contrast-to-noise ratio of the magnetization transfer weighted signal; HC, healthy, age-matched controls; LARS, Lille Apathy Rating Scale; LC, locus coeruleus; NMSS, Non-Motor Symptom Scale; PD, Parkinson's disease. [Color figure can be viewed at wileyonlinelibrary.com]

they were masked with the same LC mask used in the previous analyses and subsequently smoothed with a 1-mm full width at half maximum Gaussian kernel, after which we applied threshold-free cluster enhancement (TFCE; extent (E) = 0.5, height (H) = 2, and six neighborhood connectivity) with 10,000 permutations to correct for multiple comparisons and included age as a regressor of no interest.³⁷ Inference on TFCE statistics were restricted to voxels within the LC mask. The motivation behind masking and smoothing was to allow us to examine spatial distributions of signal loss while preserving sensitivity in the analysis.

In an exploratory analysis, we identified distributed patterns in the CNR_{MTW}-maps over the LC search space using principal component analysis (PCA). To this end, we z scored CNR_{MTW}-maps and applied PCA across participants. We focused on the three first components that explained most variance in the data (52.7% variance explained). We assessed between-group differences in principal component (PC) loadings for each PC using two-tailed independent-samples

t tests and investigated if loadings correlated with clinical scores in the PD group using two-tailed Spearman rank correlations.

Results

Clinical Data

The PD group and control group did not differ in age ($z = 548, P = 0.557$) or sex ($\chi^2 = 0.471, P = 0.493$; Table 1), but patients had significantly higher BDI-II scores ($z = 263.5, P = 0.001$) and LARS scores ($t_{56.6} = -2.26, P = 0.028$) compared with HCs. Of 42 patients, 17 had orthostatic hypotension, showing a systolic pressure drop of ≥ 20 mmHg or diastolic pressure drop of ≥ 10 mmHg, as defined by the Consensus Committee of the American Autonomic Society and the American Academy of Neurology. Of these 17 patients, one met the criterion of a diastolic pressure drop of ≥ 10 mmHg, nine met the criterion of a systolic pressure drop of ≥ 20 mmHg, and seven had both systolic and

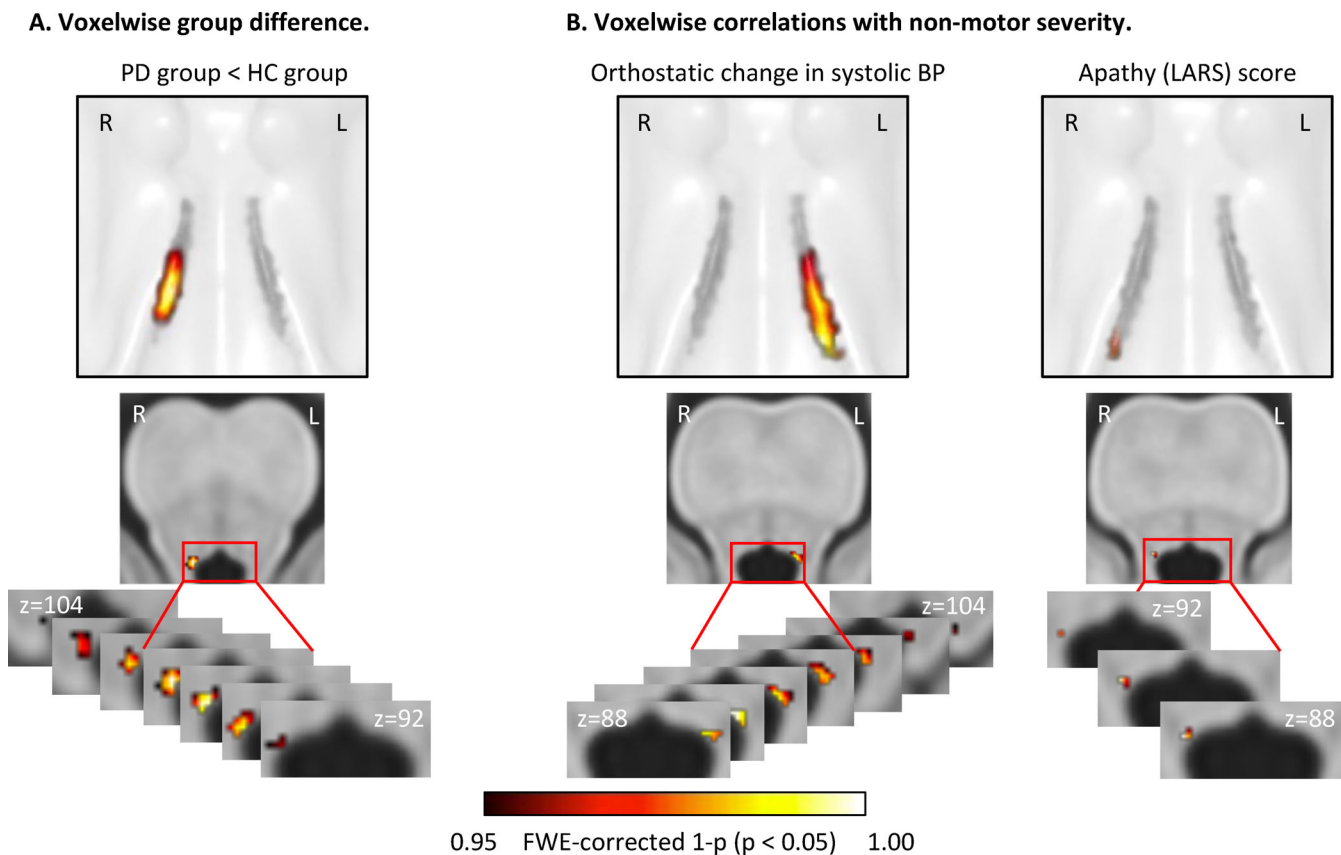


FIG. 3. Voxelwise differences in LC CNR_{MTW} and correlations with nonmotor symptom severity. Between-group difference in LC CNR_{MTW} was assessed voxelwise by applying threshold-free cluster enhancement. Patients had reduced CNR_{MTW} in a cluster of voxels in the right caudal LC (A). Voxelwise correlation with nonmotor symptom severity was assessed in the PD group. Orthostatic change in systolic BP correlated with CNR_{MTW} values in a cluster in the left caudal LC, and apathy correlated negatively in a cluster in the right caudal LC (B). Correlations were tested with age as a regressor of no interest. Maps are thresholded at FWE-adjusted $P < 0.05$. Top panels visualize the locations of significant clusters on interpolated three-dimensional renderings. BP, blood pressure; CNR_{MTW}, contrast-to-noise ratio of the magnetization transfer weighted signal; FWE, family-wise error rate; HC, healthy, age-matched controls; L, left; LARS, Lille Apathy Rating Scale; LC, locus coeruleus; PD, Parkinson’s disease; R, right. [Color figure can be viewed at wileyonlinelibrary.com]

diastolic pressure drop above the limits. Two HCs were treated with antihypertensive treatments in the form of β -1-receptor antagonists, and nine patients were on antihypertensive treatments, including β -1-receptor antagonists ($n = 4$), diuretics ($n = 3$), and angiotensin-converting enzyme inhibitors or calcium channel blockers ($n = 3$) as either monotherapy ($n = 2$) or in combination ($n = 7$).

Structural Disintegration of the LC

Patients had lower mean CNR_{MTw} values in the right LC than the HCs ($t_{57.2} = -2.96, P = 0.002$), whereas the left LC CNR_{MTw} values were not significantly different from the HCs ($t_{62.7} = -0.69, P = 0.25$). The group data are illustrated in Figure 1A. We found no significant correlations between mean CNR_{MTw} in the LC and the severity of overall nonmotor symptoms (NMSS). Mean CNR_{MTw} values in left LC correlated positively with the orthostatic drop in systolic blood pressure (Fig. 1C). Patients with low mean CNR_{MTw} values in the left LC exhibited larger systolic blood pressure decreases than patients with high mean CNR_{MTw} values ($\rho = 0.42$, uncorrected $P = 0.003$, FWE-corrected $P = 0.037$). This inverse relationship was still significant after the exclusion of patients receiving antihypertensive treatment (Supplementary Fig. S3D). A similar trend was observed for the right

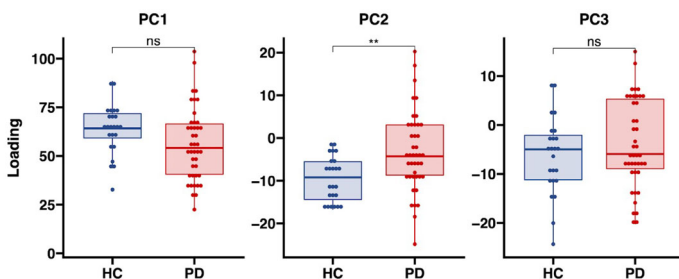
LC. Patients with low mean CNR_{MTw} values in the right LC showed a trend toward an association with higher apathy ratings. Otherwise, no significant correlations were found between the overall LC CNR_{MTw} values and other clinical variables such as depression scores, disease duration, time since symptom onset, and levodopa equivalent dose (Supplementary Fig. S3A,B).

Changes in MTw Contrast of the LC Along Its Rostro-Caudal Axis

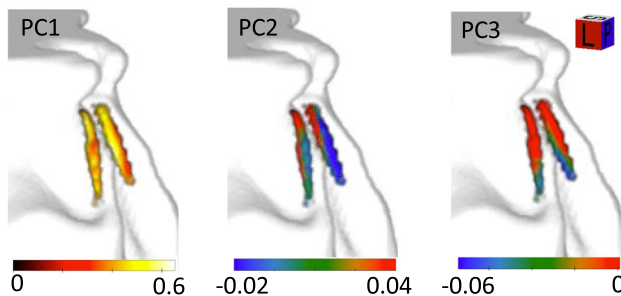
Slicewise comparison revealed that patients had lower mean CNR_{MTw} values in the caudal part of the LC than the HCs (Fig. 2A). The between-group difference was significant in the right middle and caudal LC, including slices at z coordinates 91 to 102 (FWE-adjusted $P < 0.05$; Fig. 2B). CNR_{MTw} values from slices in the left caudal LC correlated positively with orthostatic systolic blood pressure change (from z coordinates 86–96). A negative correlation between CNR_{MTw} values in the caudal LC was also observed for apathy severity, but did not survive correction for multiple comparisons (Fig. 2C).

Voxelwise analyses showed a cluster of voxels in the right caudal LC with significantly reduced CNR_{MTw} values relative to the HCs (TFCE, FWE-adjusted $P < 0.05$; cluster size: 98 voxels; Fig. 3A). A cluster in the left caudal LC showed a relationship between regional CNR_{MTw} values and orthostatic drop in

A. Group difference in principal component loadings.



B. Visualization of principal components



C. PC2 correlations with non-motor symptoms.

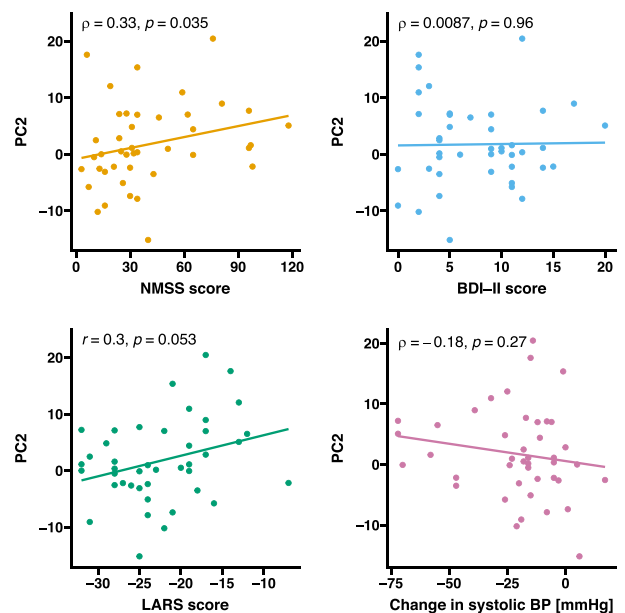


FIG. 4. Principal component analysis. Principal component analysis was applied on CNR_{MTw} maps from all participants to investigate patterns of disease-related changes in LC CNR_{MTw} . Loadings on PC2 reflecting a gradient along the rostro-caudal and dorso-ventral axes of the nucleus were different across groups (A). This gradient (visualized in B) was found to correlate with overall nonmotor symptom severity (NMSS) and a trend was observed toward a correlation with apathy (LARS), but not with depression (BDI-II score) or orthostatic change in systolic BP (C). BDI-II, Beck's Depression Inventory II; BP, blood pressure; CNR_{MTw} , contrast-to-noise ratio of the magnetization transfer weighted signal; HC, healthy, age-matched controls; LARS, Lille Apathy Rating Scale; LC, locus coeruleus; NMSS, Non-Motor Symptom Scale; ns, nonsignificant; PC1, principal component 1; PC2, principal component 2; PC3, principal component 3; PD, Parkinson's disease. [Color figure can be viewed at wileyonlinelibrary.com]

systolic blood pressure (FWE-adjusted $P < 0.05$; cluster size: 106 voxels; Fig. 3B). The lower the CNR_{MTw} values in these voxels, the higher was the drop in systolic blood pressure. In a small cluster in the right caudal LC, CNR_{MTw} values were associated with apathy severity as indexed by the LARS score (FWE-adjusted $P < 0.05$; cluster size: 10 voxels; Fig. 3C). No significant clusters were found for general nonmotor symptom severity (NMSS) or depressive symptoms (BDI-II).

Principal Component Analysis

Voxelwise PCA yielded a set of orthogonal PCs (Fig. 4B). PC1, PC2, and PC3 explained 34.84%, 9.41%, and 8.46% of the total variance, respectively. The weights of PC1 reflected a weighted sum of CNR_{MTw} over the entire LC. The spatial pattern of the PC2 weights corresponded to a combination of rostro-caudal and dorso-ventral gradients within the bilateral nuclei with negative weights in caudal and dorsal parts of the nucleus and positive weights in rostral and ventral parts. We found a significant group difference in PC2 scores with more negative mean scores in the HC group compared with the PD group ($F_{1,64} = 9.192$, FWE-adjusted $P = 0.0033$), consistent with patients having lower CNR_{MTw} values in the caudal parts of the nucleus (Fig. 4A). The group difference in PC2 scores was presumably driven by high CNR_{MTw} values in caudal-dorsal voxels relative to rostral-ventral voxels in the HCs, resulting in negative loadings in the HCs. In contrast, patients exhibited more positive loadings, presumably reflecting an attenuated rostro-caudal gradient (Supplementary Fig. S5). In the PD group, the more positive the loadings of PC2, the higher were the individual NMSS scores ($\rho = 0.33$, $P = 0.035$). A similar trend was observed toward a correlation with the LARS score ($\rho = 0.30$, $P = 0.053$; Fig. 4C).

Discussion

Using ultra-high-field MTw MRI, we were able to pinpoint how PD affects the structural integrity of the LC. Structural disintegration was not homogeneously expressed in LC, as evidenced by an accentuated CNR_{MTw} loss in its caudal part. We also found an association between regional structural disintegration and the individual expression of nonmotor symptoms. The stronger CNR_{MTw} was reduced in the left caudal LC, the larger was the orthostatic drop in blood pressure. The stronger CNR_{MTw} was reduced in the right caudal LC, the higher were patients' apathy ratings.

Overall Reduction of the Neuromelanin-Sensitive Signal in the LC

The reduction of mean LC CNR_{MTw} in PD confirms previous MRI studies performed at high field strength

and has also been shown in patients with RBD who are at high risk of developing PD.^{11,15,16,20,22,38} This robust and replicable reduction of LC contrast on neuromelanin-sensitive MRI images provides an in vivo indication of the loss of pigmented LC neurons demonstrated in postmortem histological studies.^{10,39-41} In our study as well as previous neuroimaging studies, the attenuation of CNR_{MTw} did not correlate with disease duration or motor severity. Accordingly, 16 of 17 postmortem studies failed to show an association between LC neuronal loss and disease duration.^{41,42} Therefore, we conclude that neuromelanin-sensitive MRI of the LC captures an aspect of PD-related neurodegeneration, which does not scale with disease duration or motor severity and is not attributable to dopaminergic neuronal loss and nigrostriatal dysfunction.

Spatial Gradient of Signal Loss in the LC

Voxelwise and slicewise analyses showed a clear rostro-to-caudal gradient in CNR_{MTw} . CNR_{MTw} was only consistently reduced in the caudal parts of the LC, especially on the right side relative to the HCs. This is in agreement with a recent high-field MRI study in which contrast was attenuated in patients with PD in the middle and caudal parts of the LC, but not the rostral part.⁴³ A recent ultra-high-field MRI study reported the same spatial attenuation of CNR_{MTw} in slices and voxels of the caudal part of the LC.⁴⁴ PCA identified a bilaterally expressed spatial component of CNR_{MTw} values that was more weakly expressed in patients. This component was characterized by a gradient in CNR_{MTw} along the rostro-caudal and dorso-ventral axes of the nucleus. Together, these MRI findings provide converging evidence that the PD-related structural alterations revealed by neuromelanin-sensitive MRI are more pronounced in the caudal parts of the LC characterized by a low density of neuromelanin-containing neurons.⁴⁵ This notion contrasts with postmortem studies mostly reporting a uniform neuronal loss over the entire LC,^{39,40,46-48} although some postmortem studies reported some degree of spatial inhomogeneity with greater neuronal loss in the middle and caudal parts.^{39,40,42} A possible explanation for this apparent discrepancy between MRI and histopathologic findings is that CNR_{MTw} may not only be affected by the magnitude of cell loss but also by dysfunctional neuromelanin-positive cells that have not yet undergone apoptosis. Unexpectedly, we found an asymmetry in LC CNR_{MTw} in both patients and HCs, with participants having lower values in the left hemisphere. We attribute this finding to a left-right field inhomogeneity.

Structure-Function Relationship

The clusters in the caudal LC showing the strongest attenuation in CNR_{MTw} coincided with clusters that showed a structure-dysfunction relationship for specific

nonmotor symptoms. The demonstration of an association between neuromelanin MRI contrast and specific nonmotor symptoms in PD extends previous MRI work showing a link between the neuromelanin-sensitive MRI signal in LC and RBD, mild cognitive impairment, and depressive symptoms.^{12,14,15} Our finding that a low CNR_{MTw} in the right caudal LC scales with the individual expression of apathy confirms and extends a recent 7T MRI study showing a correlation between LC integrity and apathy in a pooled cohort of patients with PD and progressive supranuclear palsy.⁴⁴ Together, these findings support a role of noradrenergic dysfunction in the development of apathy in PD, which needs to be elucidated in future studies.

The positive correlation between attenuated CNR_{MTw} in the left caudal LC and orthostatic drop in systolic blood pressure in patients with PD is a novel finding, extending previous lines of research into noradrenergic dysfunction in PD. A recent PET study found that the distribution volume ratio of the noradrenaline transporter PET-tracer 11C-methylreboxetine (MeNER) in the LC and hypothalamus correlated with orthostatic change in systolic blood pressure, but only when including healthy participants in the analysis.¹⁵ In support of our finding, a neuromelanin-sensitive MRI study performed in healthy participants found a negative correlation between LC contrast and high-frequency heart rate variability in older adults.⁴⁹ The association of loss of LC integrity, noradrenergic dysfunction and orthostatic hypotension, and abnormal heart rate variability could be explained by a loss of LC-mediated inhibition of the parasympathetic modulation of the heart by the vagus nerve.⁵⁰⁻⁵² Co-occurrence of the degeneration of LC neurons and peripheral postganglionic sympathetic neurons^{53,54} could also explain the association with orthostatic hypotension. Taken together, these findings support the notion that noradrenergic neurodegeneration in LC makes a critical contribution to the development of orthostatic hypotension in PD.

Finally, recent studies in patients with Alzheimer's disease and PD suggest that LC degeneration might be associated with cognitive impairment in these neurodegenerative disorders.^{55,56} We did not plan to investigate this association and did not collect any data on cognitive performance apart from the Montreal Cognitive Assessment (MoCA). Unfortunately, we did not observe any relationship between MoCA scores and CNR_{MTw} of the LC (Supplementary Fig. S6). Furthermore, we did not observe any relationship between LC CNR_{MTw} and motor severity (Supplementary Fig. S6). Disintegration of the LC has been shown to be present in individuals with RBD.^{11,15} Unfortunately, we did not include clinical measures of RBD in our study, and thus it was impossible to assess the relationship between RBD and LC disintegration in our study."

Strengths and Limitations

A strength of this study is the use of tailored data acquisition and analysis protocols. First, the high in-plane spatial resolution of the MTw images minimized partial volume effects. Second, we leveraged a coregistration and normalization procedure published by Ye and colleagues (Supplementary Fig. S7),³⁴ which secures accurate coregistration and normalization, and visually verified that normalization results were accurate. This is critical as the LC is a small nucleus and even minor normalization and coregistration errors can introduce undesired variability in the results. Third, we excluded hyperintense voxels at the border of the fourth ventricle that do not belong to the LC.

The neurobiological mechanisms contributing to neuromelanin MRI contrast is a matter of ongoing debate.^{25,57,58} Furthermore, MTw MRI is not specific to neuromelanin-rich structures, and hyperintensity is also observed in the periaqueductal gray, which has low neuromelanin content.⁵⁹ It is therefore important to note that although the contrast on neuromelanin-sensitive MRI likely reflects the number of neuromelanin-positive LC neurons,²⁴ attenuation of CNR_{MTw} might not reflect the magnitude of LC neuronal loss or noradrenergic denervation of LC targets. Our MTw acquisition had limited spatial resolution in the slice direction, which could lead to partial volume effects in extreme ends of the nucleus. CNR was consistently higher in the right LC compared with the left LC, and mean CNR_{MTw} values were only significantly lower in the right LC in patients. The notion of a right-left asymmetry is not supported by postmortem studies.^{40,45,60,61} Spatial variations in the B1-field between vendors may account for this apparent asymmetry. Previous neuroimaging studies have found a similar asymmetry with higher right LC contrast in studies using Philips scanners and higher left LC contrast in studies using Siemens scanners.^{58,62-64} This right-left asymmetry in neuromelanin-sensitive contrast might have limited the sensitivity to detect a between-group difference in the left LC.

Antihypertensive treatment was not withdrawn before blood pressure measurements. Excluding patients on antihypertensive treatment did not influence our conclusions regarding the association between LC contrast and orthostatic systolic blood pressure change.

Conclusion

Our results show that neuromelanin-sensitive MTw MRI at ultra-high-field strength can map spatial gradients of structural disintegration in the LC, showing a preferential involvement of the caudal portion of LC in PD and a clear relationship between reduced structural integrity of caudal LC and orthostatic dysregulation and apathy. ■

Acknowledgments: We thank Dr. Rong Ye and Professor James B. Rowe from the Department of Clinical Neurosciences, University of Cambridge and Cambridge University Hospitals NHS Foundation Trust for kindly sharing their probabilistic atlas of the locus coeruleus and for providing support in setting up the image postprocessing pipeline. We would also like to thank the patients and healthy participants who participated in our study.

Data Availability Statement

The data that support the findings of this study are available from the corresponding author upon reasonable request.

References

- Schapira AHV, Chaudhuri KR, Jenner P. Non-motor features of Parkinson disease. *Nat Rev Neurosci* 2017;18:435–450.
- Goldstein DS. Orthostatic hypotension as an early finding in Parkinson's disease. *Clin Auton Res* 2006;16:46–54.
- den Brok MGHE, van Dalen JW, van Gool WA, van Charante EPM, de Bie RMA, Richard E. Apathy in Parkinson's disease: a systematic review and meta-analysis. *Mov Disord* 2015;30:759–769.
- Reijnders JSAM, Ehrt U, Weber WEJ, Aarsland D, Leentjens AFG. A systematic review of prevalence studies of depression in Parkinson's disease. *Mov Disord* 2008;23:183–189.
- Kaalund SS, Passamonti L, Allinson KSJ, et al. Locus coeruleus pathology in progressive supranuclear palsy, and its relation to disease severity. *Acta Neuropathol Commun* 2020;8:11
- Theofilas P, Ehrenberg AJ, Dunlop S, et al. Locus coeruleus volume and cell population changes during Alzheimer's disease progression: a stereological study in human postmortem brains with potential implication for early-stage biomarker discovery. *Alzheimers Dement J Alzheimers Assoc* 2017;13:236–246.
- Poe GR, Foote S, Eschenko O, et al. Locus coeruleus: a new look at the blue spot. *Nat Rev Neurosci* 2020;21:644–659.
- Sara SJ. The locus coeruleus and noradrenergic modulation of cognition. *Nat Rev Neurosci* 2009;10:211–223.
- Braak H, del Tredici K, Rüb U, de Vos RAI, Jansen Steur ENH, Braak E. Staging of brain pathology related to sporadic Parkinson's disease. *Neurobiol Aging* 2003;24:197–211.
- Zarow C, Lyness SA, Mortimer JA, Chui HC. Neuronal loss is greater in the locus coeruleus than nucleus basalis and substantia nigra in Alzheimer and Parkinson diseases. *Arch Neurol* 2003;60:337–341.
- Ehrminger M, Latimier A, Pyatigorskaya N, et al. The coeruleus/subcoeruleus complex in idiopathic rapid eye movement sleep behaviour disorder. *Brain* 2016;139:1180–1188.
- García-Lorenzo D, Longo-Dos Santos C, Ewencyk C, et al. The coeruleus/subcoeruleus complex in rapid eye movement sleep behaviour disorders in Parkinson's disease. *Brain* 2013;136:2120–2129.
- Isaias IU, Trujillo P, Summers P, et al. Neuromelanin imaging and dopaminergic loss in Parkinson's disease. *Front Aging Neurosci* 2016;8:196
- Li Y, Wang C, Wang J, et al. Mild cognitive impairment in de novo Parkinson's disease: a neuromelanin MRI study in locus coeruleus. *Mov Disord* 2019;34:884–892.
- Sommerauer M, Fedorova TD, Hansen AK, et al. Evaluation of the noradrenergic system in Parkinson's disease: an 11C-MeNER PET and neuromelanin MRI study. *Brain* 2018;141:496–504.
- Wang J, Li Y, Huang Z, et al. Neuromelanin-sensitive magnetic resonance imaging features of the substantia nigra and locus coeruleus in de novo Parkinson's disease and its phenotypes. *Eur J Neurol* 2018;25:949–e73.
- Aston-Jones G, Ennis M, Pieribone VA, Nickell WT, Shiple MT. The brain nucleus locus coeruleus: restricted afferent control of a broad efferent network. *Science* 1986;234:734–737.
- Loughlin SE, Foote SL, Grzanna R. Efferent projections of nucleus locus coeruleus: morphologic subpopulations have different efferent targets. *Neuroscience* 1986;18:307–319.
- Mason ST, Fibiger HC. Regional topography within noradrenergic locus coeruleus as revealed by retrograde transport of horseradish peroxidase. *J Comp Neurol* 1979;187:703–724.
- Castellanos G, Fernández-Seara MA, Lorenzo-Betancor O, et al. Automated neuromelanin imaging as a diagnostic biomarker for Parkinson's disease. *Mov Disord* 2015;30:945–952.
- Sasaki M. Monoamine neurons in the human brain stem: anatomy, magnetic resonance imaging findings, and clinical implications. *NeuroReport* 2008;19:1649–1654.
- Sasaki M, Shibata E, Tohyama K, et al. Neuromelanin magnetic resonance imaging of locus coeruleus and substantia nigra in Parkinson's disease. *Neuroreport* 2006;17:1215–1218.
- O'Callaghan C, Hezemans FH, Ye R, et al. Locus coeruleus integrity and the effect of atomoxetine on response inhibition in Parkinson's disease. *Brain* 2021;144(8):2513–2526.
- Keren NI, Taheri S, Vazey EM, et al. Histologic validation of locus coeruleus MRI contrast in post-mortem tissue. *NeuroImage* 2015;113:235–245.
- Priovoulos N, Jacobs HIL, Ivanov D, Uludag K, Verhey FRJ, Poser BA. High-resolution in vivo imaging of human locus coeruleus by magnetization transfer MRI at 3T and 7T. *NeuroImage* 2018;168:427–436.
- Postuma RB, Berg D, Stern M, et al. MDS clinical diagnostic criteria for Parkinson's disease. *Mov Disord* 2015;30:1591–1601.
- Chaudhuri KR, Healy DG, Schapira AH. Non-motor symptoms of Parkinson's disease: diagnosis and management. *Lancet Neurol* 2006;5:235–245.
- Fahn S, Elton RL, UPDRS Development Committee. The Unified Parkinson's Disease Rating Scale. *Recent Dev Park Dis.* 1987;2:153–163.
- Gibbons CH, Schmidt P, Biaggioni I, et al. The recommendations of a consensus panel for the screening, diagnosis, and treatment of neurogenic orthostatic hypotension and associated supine hypertension. *J Neurol* 2017;264:1567–1582.
- Beck AT, Ward CH, Mendelson M, Mock J, Erbaugh J. An inventory for measuring depression. *Arch Gen Psychiatry* 1961;4:561–571.
- Drijgers RL, Dujardin K, Reijnders JSAM, Defebvre L, Leentjens AFG. Validation of diagnostic criteria for apathy in Parkinson's disease. *Parkinsonism Relat Disord* 2010;16:656–660.
- Schrag A, Barone P, Brown RG, et al. Depression rating scales in Parkinson's disease: critique and recommendations. *Mov Disord* 2007;22:1077–1092.
- Sockeel P, Dujardin K, Devos D, Denève C, Destée A, Defebvre L. The Lille Apathy Rating Scale (LARS), a new instrument for detecting and quantifying apathy: validation in Parkinson's disease. *J Neurol Neurosurg Psychiatry* 2006;77:579–584.
- Ye R, Rua C, O'Callaghan C, et al. An in vivo probabilistic atlas of the human locus coeruleus at ultra-high field. *NeuroImage* 2021;225:117487
- Tustison NJ, Avants BB, Cook PA, et al. N4ITK: improved N3 bias correction. *IEEE Trans Med Imaging* 2010;29:1310–1320.
- Fonov V, Evans AC, Botteron K, Almli CR, McKinstry RC, Collins DL. Unbiased average age-appropriate atlases for pediatric studies. *NeuroImage* 2011;54:313–327.
- Smith SM, Nichols TE. Threshold-free cluster enhancement: addressing problems of smoothing, threshold dependence and localisation in cluster inference. *NeuroImage* 2009;44:83–98.
- Schwarz ST, Xing Y, Tomar P, Bajaj N, Auer DP. In vivo assessment of brainstem depigmentation in Parkinson disease: potential as a severity marker for multicenter studies. *Radiology* 2017;283:789–798.
- German DC, Manaye KF, White CL, et al. Disease-specific patterns of locus coeruleus cell loss. *Ann Neurol* 1992;32:667–676.
- Chan-Palay V, Asan E. Alterations in catecholamine neurons of the locus coeruleus in senile dementia of the Alzheimer type and in Parkinson's disease with and without dementia and depression. *J Comp Neurol* 1989;287:373–392.

41. Giguère N, Burke Nanni S, Trudeau L-E. On cell loss and selective vulnerability of neuronal populations in Parkinson's disease. *Front Neurol* 2018;9:455
42. Bertrand E, Lechowicz W, Szpak GM, Dymecki J. Qualitative and quantitative analysis of locus coeruleus neurons in Parkinson's disease. *Folia Neuropathol* 1997;35:80–86.
43. Doppler CEJ, Kinnerup MB, Brune C, et al. Regional locus coeruleus degeneration is uncoupled from noradrenergic terminal loss in Parkinson's disease. *Brain* 2021;144(9):2732–2744.
44. Ye R, O'Callaghan C, Rua C, et al. Locus coeruleus integrity from 7T MRI relates to apathy and cognition in Parkinson's disease and progressive supranuclear palsy. *medRxiv* 2021. <https://doi.org/10.1101/2021.04.19.21255762>.
45. German D, Walker B, Manaye K, Smith W, Woodward D, North A. The human locus coeruleus: computer reconstruction of cellular distribution. *J Neurosci* 1988;8:1776–1788.
46. Espay AJ, LeWitt PA, Kaufmann H. Norepinephrine deficiency in Parkinson's disease: the case for noradrenergic enhancement. *Mov Disord* 2014;29:1710–1719.
47. Kelberman M, Keilholz S, Weinshenker D. What's that (blue) spot on my MRI? Multimodal neuroimaging of the locus Coeruleus in neurodegenerative disease. *Front Neurosci* 2020;14. <https://doi.org/10.3389/fnins.2020.583421>
48. Paredes-Rodriguez E, Vegas-Suarez S, Morera-Herreras T, de Deurwaerdere P, Miguez C. The noradrenergic system in Parkinson's disease. *Front Pharmacol* 2020;11. <https://doi.org/10.3389/fphar.2020.00435>
49. Mather M, Joo Yoo H, Clewett DV, et al. Higher locus coeruleus MRI contrast is associated with lower parasympathetic influence over heart rate variability. *NeuroImage* 2017;150:329–335.
50. Elam M, Svensson TH, Thoren P. Differentiated cardiovascular afferent regulation of locus coeruleus neurons and sympathetic nerves. *Brain Res* 1985;358:77–84.
51. Wang X, Piñol RA, Byrne P, Mendelowitz D. Optogenetic stimulation of locus Coeruleus neurons augments inhibitory transmission to parasympathetic cardiac vagal neurons via activation of brainstem $\alpha 1$ and $\beta 1$ receptors. *J Neurosci* 2014;34:6182–6189.
52. Wood CS, Valentino RJ, Wood SK. Individual differences in the locus coeruleus-norepinephrine system: relevance to stress-induced cardiovascular vulnerability. *Physiol Behav* 2017;172:40–48.
53. Braak H, Sastre M, Bohl JRE, de Vos RAI, del Tredici K. Parkinson's disease: lesions in dorsal horn layer I, involvement of parasympathetic and sympathetic pre- and postganglionic neurons. *Acta Neuropathol (Berl)* 2007;113:421–429.
54. Courbon F, Brefel-Courbon C, Thalamas C, et al. Cardiac MIBG scintigraphy is a sensitive tool for detecting cardiac sympathetic denervation in Parkinson's disease. *Mov Disord* 2003;18:890–897.
55. Betts MJ, Cardenas-Blanco A, Kanowski M, et al. Locus coeruleus MRI contrast is reduced in Alzheimer's disease dementia and correlates with CSF A β levels. *Alzheimers Dement* 2019;11:281–285.
56. Prasuhn J, Prasuhn M, Fellbrich A, et al. Association of locus coeruleus and substantia nigra pathology with cognitive and motor functions in patients with Parkinson disease. *Neurology* 2021;97:e1007–e1016.
57. Trujillo P, Summers PE, Ferrari E, et al. Contrast mechanisms associated with neuromelanin-MRI. *Magn Reson Med* 2017;78:1790–1800.
58. Trujillo P, Petersen KJ, Cronin MJ, et al. Quantitative magnetization transfer imaging of the human locus coeruleus. *NeuroImage* 2019;200:191–198.
59. Cassidy CM, Zucca FA, Girgis RR, et al. Neuromelanin-sensitive MRI as a noninvasive proxy measure of dopamine function in the human brain. *Proc Natl Acad Sci* 2019;116:5108–5117.
60. Mouton PR, Pakkenberg B, Gundersen HJG, Price DL. Absolute number and size of pigmented locus coeruleus neurons in young and aged individuals. *J Chem Neuroanat* 1994;7:185–190.
61. Ohm TG, Busch C, Bohl J. Unbiased estimation of neuronal numbers in the human nucleus coeruleus during aging. *Neurobiol Aging* 1997;18:393–399.
62. Betts MJ, Cardenas-Blanco A, Kanowski M, Jessen F, Düzel E. In vivo MRI assessment of the human locus coeruleus along its rostrocaudal extent in young and older adults. *NeuroImage* 2017;163:150–159.
63. Liu KY, Acosta-Cabronero J, Cardenas-Blanco A, et al. In vivo visualization of age-related differences in the locus coeruleus. *Neurobiol Aging* 2019;74:101–111.
64. Tona K-D, Keuken MC, de Rover M, et al. In vivo visualization of the locus coeruleus in humans: quantifying the test-retest reliability. *Brain Struct Funct* 2017;222(9):4203–4217.

Supporting Data

Additional Supporting Information may be found in the online version of this article at the publisher's web-site.